# Photodissociation via weak intersystem crossing: Incoherent versus coherent excited-state nonadiabatic dynamics in math xmlns="http://www.w3.org/1998/Math/MathML">msub>mi mathvariant="normal">N/mi>mn>2/mn>/msub>/math>

Natalia Gelfand, Ksenia Komarova, Francoise Remacle, and Raphael D. Levine

Phys. Rev. A **108**, 053116 — Published 17 November 2023

DOI: 10.1103/PhysRevA.108.053116

# Photodissociation via weak intersystem crossing: incoherent vs. coherent excited-state nonadiabatic dynamics in $N_2$

Natalia Gelfand,[1*] Ksenia Komarova,[1] Francoise Remacle,[1,2] and Raphael D. Levine[1,3,4]

[1] The Fritz Haber Center for Molecular Dynamics, Institute of Chemistry, The Hebrew University of Jerusalem, Jerusalem 91904, Israel

[2] Theoretical Physical Chemistry, UR MolSys B6c, University of Liège, B4000 Liège, Belgium

[3] Department of Molecular and Medical Pharmacology, David Geffen School of Medicine and

[4] Department of Chemistry and Biochemistry, University of California, Los Angeles, CA 90095, USA

*natalia.gelfand@mail.huji.ac.il

Abstract.

Vacuum UV light at a well-defined wavelength excites $N_2$ to different vibronic levels of the singlet electronic states that strongly interact through non adiabatic coupling. Each discrete vibronic state acts as an isolated resonance: it is weakly coupled to a dissociative continuum of triplet states via a weak spin-orbit coupling. Here we seek to compare this decay to that of a coherent superposition of bound singlets pumped by a broad in energy – ultrafast pulse. Despite the strong inter-singlets and inter-triplets nonadiabatic couplings, the coherent set of states decays as a *mixture* of the isolated vibronic states with essentially their individual lifetimes as determined separately in a sharp wavelength excitation. The vibrational quantum number of the vibronic states is a nearly good one when the spin-orbit coupling is as weak as is the case for $N_2$. Numerically converged dynamical computations valid for longer times show that for non-rotating molecules the individual vibronic resonances overlap and interfere only upon an artificially order of magnitude increase of the strength of the spin-orbit coupling. The resonances strongly overlap only at an even stronger coupling to the dissociative continuum.

# I.INTRODUCTION

At higher energies molecules have a dense spectrum that often cannot be well characterized by good quantum numbers. This mixing of states is primarily due the strong coupling induced by the breakdown of the Born-Oppenheimer separation of electronic and nuclear dynamics and, in polyatomics, by resonance coupling of normal modes due to anharmonicities. States of well-defined character are thereby typically entangled resulting in a coherent superposition of allied states. By coherence we here mean the special quantum mechanical linear superposition relation of otherwise stationary states that is relevant to systems of many and closely spaced levels. Such a coherent state evolves in time in an oscillatory manner where the relevant frequencies are the energy gaps between the participating states. Different spectroscopies can therefore create and/or probe coherences of different character. The slower are coherences in the microwave range as studied in NMR [1,2] through IR for rotational states [3,4] or for higher Rydberg electronic states [5,6]. In the near IR/visible range is the coherence of vibrational states [7-10]. Excited electronic states can each carry a rich manifold of vibrotational states that can be coherently pumped [11]. In this paper we deal with the currently fastest oscillating coherences due to electronic states accessed by fast, few femtoseconds pulses [12-14]. Our concrete example is the diatomic molecule $N_2$ [15-18] that even in its lowest optically reachable excited states is a mix of electronic states of definite character.

To define a vibrational basis, we here first diagonalize the electronic Hamiltonian using quantum chemical methods. This generates an adiabatic electronic basis that is dependent on the internuclear distance $R$. We next diagonalize the full Hamiltonian in this adiabatic basis. The full Hamiltonian matrix contains the off-diagonal terms that couple different adiabatic states, terms that are known as the nonadiabatic couplings. The result is that each vibrational state is associated with a coherent linear superposition of adiabatic electronic states. In a fast excitation one can readily pump a coherent superposition of these vibronic states.

We can proceed differently to the diagonalization of the Hamiltonian. We first use quantum chemistry to introduce a diabatic electronic basis. Here each electronic state has a definite character [19-21]. These states are assumed to be only slowly varying with the interatomic distance $R$. They are coupled by electronic off-diagonal potentials that are functions of $R$. One can also diagonalize the total Hamiltonian in this basis. The vibrational states and their spectrum are essentially the same as in the alternative method above. Following an attosecond excitation also the diabatic states beat against one another [16]. Indeed the exchange of

population occurs at much the same time ranges, i.e., when the vibrational wave packets overlap in the region of coupling, see, for example, Fig. 5 in [22]. It is therefore possible to experimentally detect the coherence of the electronic states [12,13,23].

In the nitrogen molecule, the electronic states of the same symmetry interact strongly due to large off-diagonal coupling terms and thus each vibrational level is a coherent superposition of a few electronic states represented in either adiabatic or diabatic basis. The chosen basis does not affect the energy of the vibronic states, just the composition of each eigenstate will reflect the difference between the bases. The following discussion will be given in the adiabatic representation which is the direct result of quantum chemical calculations.

The optically accessible excited $^1\Sigma_u^+$ states of the $N_2$ molecule are well apart from its ground state $X^1\Sigma_g^+$ by almost 12 eV which makes these states accessible under vacuum ultraviolet (VUV) one-photon excitation. Three adiabatic $^1\Sigma_u^+$ singlet states are shown in Fig. 1a with colored lines. These singlets are bound for the excitation energies below 116,000 $cm^{-1}$, and so the energy rich $N_2$ molecule dissociates indirectly by a weak and localized spin-orbit coupling of the singlet states to the triplet and then quintet states which are shown in Fig. 1a in dark grey color. Our quantum chemical calculations predicted the coupling between $^1\Sigma_u^+$ and $^3\Pi_u$ states to be of the order of 30 $cm^{-1}$ at most. This makes the total population in the singlet states decay slowly, varying non-monotonically in energy from hundreds down to tens of picoseconds.

The independent of one another decay of the singlet vibronic states is as expected for isolated meaning not overlapping resonances [24]. Our singlet states are not trapped [25] because of the sparsity of the continuum but decay through a narrow bottleneck [26] to a dense and strongly mixed continuum. There are two main exit channels accessible in the triplet manifold and each is coupled to the singlets at different internuclear distances. The spin-orbit coupling of the vibronic states to the continuum is weak and smaller than their spacing so they are uncoupled via the triplets and act as isolated resonances. Indeed, high resolution optical spectroscopy typically resolves even the rotational states of a given vibronic state [27,28]. The non-monotonic variation of the lifetimes of the singlets as a function of energy can be interpreted in terms of the complexity of the nonadiabatic couplings of the different triplet states, see Fig. 4 of [29]. In the present study we also examine how this complexity can be reflected in the coherent dynamics.

There has been important interest in the key differences in the dynamics between a fast laser and a slow, sunlight like, natural incoherent excitation [30-33]. In this paper we compare the results for an ultrafast excited molecule to the earlier work on predissociation dynamics of individually excited vibrational states using a long laser pulse [15,29]. Both the short and long duration pulses are Gaussians that are transform limited in a manner that insures that there is no source term in the Fourier transform. The pulse of short duration coherently spans about a dozen single vibrational eigenstates. The pulse of long duration is chosen so that it excites essentially just a single eigenstate, and it is about 50-fold longer than the short pulse. The earlier work was undertaken to compare with experimental results on the distribution of exit channels in VUV excited $N_2$ [34-36]. In the present work, we aim to elucidate the role of a not stationary initial state on the photodissociation dynamics in $N_2$ that follows upon excitation by a laser pulse that is wide in energy.

## II. THEORETICAL OVERVIEW

### *Selection rules*

Here we briefly discuss the rules important for understanding population transfer in the $N_2$ molecule, a more detailed explanation of selection rules can be found in [37]. The homonuclear $N_2$ molecule belongs to $D_{\infty h}$ point group and therefore all its electronic states can be classified either 'gerade' or 'ungerade' relative to the inversion operation. In the present paper, we discus one photon VUV excitation of $N_2$ from its ground state $X^1\Sigma_g^+$. The dipole allowed transitions are those with the change of parity that means only $^1\Sigma_u^+$ and $^1\Pi_u$ can be optically accessed with one photon. We assume that the molecule is aligned along its Z axis and so the $^1\Sigma_u^+$ states will be populated exclusively. These states are coupled to other 'ungerade' states of higher multiplicity via spin-orbit coupling. There are three Cartesian components of the spin-orbit coupling integrals, along X, Y and Z axes in the molecular frame. For LSZ coupling the two interacting states should have the same magnetic quantum number, $\Delta m_s = 0$, where $m_s$, is the projection of $S$ on the internuclear axis. For LSX/LSY coupling $\Delta m_s = \pm 1$. $^1\Sigma_u^+$ singlet states are coupled by LSX/LSY spin-orbit interaction to the $^3\Pi_u$ states and only $m_s = \pm 1$ of the triplet states can be populated. $^1\Sigma_u^+$ are also coupled by LSZ spin-orbit interaction to the $^3\Sigma_u^-$ states and for this type of coupling the selection rule is $\Delta m_s = 0$. The same is applied to the quintets: LSZ spin-orbit interaction to the $^3\Pi_u$ and LSX/LSY spin-orbit coupling to the $^3\Sigma_u^-$. A schematic representation of these interstate relation is shown in Fig. S1 of the Supplemental Material (SM) and description for an extended basis set is given in [38]. The states of the same symmetry and multiplicity are coupled by nonadiabatic interaction and they can exchange population among themselves especially in the avoided crossings regions.

In the present study, we discuss results for the rotational level J=0 for each considered vibrational level of $N_2$. This is warranted by the experimental results that show limited J-dependence of the dissociation branching fraction at low J's. Furthermore, the high-resolution spectrum shows limited perturbation at low J's.

### *Quantum chemical and quantum dynamical computations*

To explore the photodissociation of $N_2$, we employ a fully quantum mechanical propagation technique [16] where the time-dependent Schrödinger equation is solved numerically at each internuclear coordinate of the non-rotating molecule from the region of its excitation to a dissociation limit. Propagating in such manner, we include electron-nuclear interactions, such as nonadiabatic and spin-orbit couplings computed *ab initio* using high-level quantum chemistry methods: a state-averaged complete active space self-consistent field (CASSCF) [39-41] approach followed by multi-reference configuration interaction (MRCI) [42,43]. In all the computations an active space of 17 orbitals (4σu, 3σg, 4πu, 4πg, and 2δg) for 10 valence electrons is employed. The two lowest 1σu and 1σg orbitals are not included in the active space but are fully optimized in the CASSCF procedure. Restriction of only single occupancy for the higher Rydberg orbitals is used. We use a doubly augmented cc-pVQZ atomic basis set with additional bond-centred s and p diffuse functions for a proper description of Rydberg and valence singlet and triplet states. The non-adiabatic couplings are calculated using the finite difference approach for MRCI wave functions as implemented in the DDR program of MOLPRO [44]. The step for the finite difference computation was optimized to get a convergence in the values of NAC, see [38] for more details. In the calculations of the spin-orbit coupling terms the averaging over the coupled states is employed. Spin-orbit coupling integrals are evaluated for the MRCI wave functions with the Breit-Pauli spin-orbit operator as implemented in MOLPRO.[45] All the quantum chemistry calculations are performed with the MOLPRO program [46]. Accuracy of the resulted potentials and couplings of the optically accessible singlet $^1\Sigma_u^+$ states is discussed in details in [38]; there also all the computed data can be found in the digital format.

The multi-electronic state wave function defined on the grid of internuclear coordinate, *R*, is propagated according to the time-dependent Schrodinger equation of motion in the basis of 9 excited electronic states: three $^1\Sigma_u^+$, four $^3\Pi_u$, one $^3\Sigma_u^-$, and one $^5\Pi_u$. The equation of motion for the amplitudes $C_{nj} = \Psi_n(R_j)$ at a given electronic state *n* and grid point $j : R = R_j$ is given as follows:

$$i\hbar\frac{dC_{nj}}{dt} = (T^d + V_n(R_j))C_{nj} - iV_{CAP}(R_j)C_{nj} + \sum_{q=1}^{2} T_q^{off}\,(C_{n,j+q} + C_{n,j-q})$$
$$-\sum_{k=1}^{N_e}\sum_{q=1}^{2} p_q\left(\left(\tau_{nk}(R_j) + \tau_{nk}(R_{j-q})\right)C_{k,j-q} - \left(\tau_{nk}(R_j) + \tau_{nk}(R_{j+q})\right)C_{k,j+q}\right) \qquad (1)$$
$$-\sum_{k=1}^{N_e}\left(E(t)\mu_{nk}(R_j) + \frac{1}{2m}\sum\nolimits_l \tau_{nl}(R_j)\cdot\tau_{lk}(R_j) - H_{nk}^{SO}(R_j)\right)C_{kj}$$

Here $T^d$ and $T_q^{off}$ are diagonal and off-diagonal kinetic energy terms, respectively, evaluated within the five-point finite difference approximation, see Ref.[16]. $V_n(R)$ denotes potential energy of an electronic state *n*. At large internuclear distances, $R > 6.2$ a.u., a complex absorbing potential, $V_{CAP}(R) = 0.01\cdot(R-6.2)^3$, is applied for all the dissociative states. The non-adiabatic couplings $\tau_{nk}(R)$ between electronic states *n* and *k* are scaled by the momentum terms, $p_q$.[47-50]. The propagation of the equation (1) is solved via the Runge-Kutta method [51] with a time step of $\Delta t$ =$10^{-4}$ fs and $\Delta R$ = 0.005 a.u. for the grid spacing. The propagation lasted for 3 ps in all the dynamical calculations.

The lifetimes of the excited vibrational singlet states are estimated by a linear fit for the logarithm of their time-dependent population, $\left|C_{nj}(t)\right|^2$, assuming a unimolecular exponential decay.

### *Parameters of the laser pulses*

The interaction with the light field is governed by the transition dipole moment $\mu_{nk}(R)$ between the ground $X^1\Sigma_g^+$ and $^1\Sigma_u^+$ excited singlet electronic states. Explicit time-profile for the VUV light field is used:

$$E(t) = \boldsymbol{\varepsilon}_p \cdot E_{\max} \cdot \exp\left(-(t-t_p)^2/2\sigma_p^2\right)[\cos(\omega_p t) - \left(\frac{t-t_p}{\omega_p\sigma_p^2}\right)\sin(\omega_p t)] \qquad (2)$$

Here $\boldsymbol{\varepsilon}_p$ is the polarization direction of the light field, set along the internuclear axis so as to access the $^1\Sigma_u^+$ states; $E_{\max}$ is the maximum amplitude of the field; $t_p$ and $\sigma_p$ are the time at which the pulse is centered and the width of the Gaussian envelope of the field.

Two sets of settings were used to mimic coherent and incoherent excitation. To excite the N2 molecule incoherently, the duration of the pulse was set to be long enough to selectively

excite specific vibrational levels of the singlet states, $\sigma_p =$ 160 fs, $t_p =$ 1200 fs and $\varepsilon_p =$ 0.0001 au. The carrier frequency $\omega_p$ was varied from 111,500 to 114,500 $cm^{-1}$ according to the energy of the vibrational levels obtained by diagonalization in the singlets manifold. The choice of this energy range was due to the availability of two dissociation channels.

Coherent excitation was established with $\sigma_p =$ 4.2 fs, $t_p =$ 35 fs, $\varepsilon_p$ = 0.001 au at frequency $\omega_p =$ 112,490 $cm^{-1}$. Such a pulse is sufficiently broad in energy to excite a bunch of vibronic singlet state: Fig. S2a of the SM shows the dipole strength distribution along with the laser pulse profile and Fig. S2b exhibits the actual vibronic singlet states distribution.

## III.RESULTS AND DISCUSSION

The ultrafast excitation is by an energy broad laser pulse from the ground state to the manifold of $^1\Sigma_u^+$ states. The pulse is centered at 112,490 cm$^{-1}$ and effectively covers the region from 111,000 to 115,000 cm$^{-1}$ (from 13.76 to 14.26 eV, see the grey area in Fig. 1a). In this energy region the singlet states are all bound and the molecule dissociates primarily through the triplet $^3\Pi_u$ manifold [17,18]. The contribution of the triplet $1^3\Sigma_u^-$ and the quintet $2^5\Pi_u$ states is orders of magnitude smaller [29], however we also include them in the dynamics.

The fast pulse lasts for 10 fs FWHM during which time $^1\Sigma_u^+$ states are populated. The $1^1\Sigma_u^+$ and $2^1\Sigma_u^+$ states are strongly mixed by nonadiabatic coupling and they are constantly exchanging population among themselves, Fig. 1b. The exchange is slower than the duration of the pulse. As soon as the singlets are getting populated, they begin transferring population to the triplets, Fig. 1c. We have earlier found the spin-orbit coupling between the singlet and triplet states to be less than 30 cm$^{-1}$ which makes the transfer to the dissociation continuum rather slow: only 0.07 % of the excited singlets go to the dissociative states during 200 fs, compare the ordinates of Fig. 1b and 1c. Figs. S3 and S4 of the SM show in addition the dynamics for the $^1\Sigma_u^+$ and $^3\Pi_u$ states at longer time scale. The triplet states are coupled by nonadiabatic terms among themselves with a fast exchange and the second triplet, $2\,^3\Pi_u$ state, is the one that is most populated throughout the propagation. There is hardly any backtransfer from the triplets to the singlets and this remains so even upon an order of magnitude increase in the strength of the fast pulse. On the other hand, as will be discussed below, considerably increasing the strength of the spin-orbit coupling enhances the exchange.

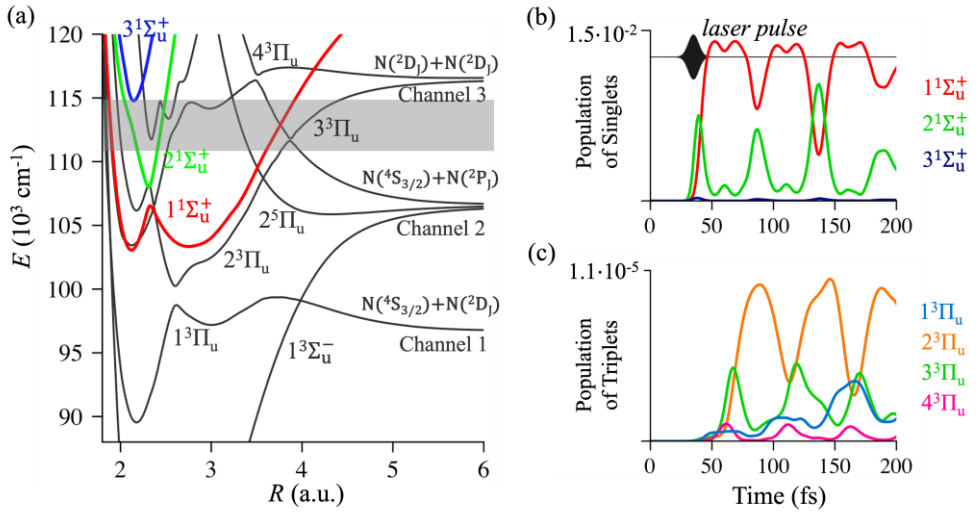


FIG. 1. Energetics and dynamics of fast pumping of $N_2$ in the VUV. (a) Potential energy curves of adiabatic electronic states included in the Hamiltonian: optically accessible singlet $^1\Sigma_u^+$ states are shown in red, green, and blue colors and dissociative states of higher multiplicity are in dark grey. The energy range discussed in the paper is marked as the gray shade. (b) Short time evolution of adiabatic singlet excited $^1\Sigma_u^+$ states with the profile of the ultrafast pulse indicted (black line) and (c) population of the triplet $^3\Pi_u$ states up to 200 fs.

Not only at early times but throughout the propagation, the vibrational quantum number is a relatively robust one. In the time-independent eigenstate picture this is seen by the rather low contribution of $^3\Pi_u$ states to eigenstates in the discussed energy range. There is an exception as shown in Fig. S5a of the SM where at an energy of a very rapidly dissociating singlet the contribution is higher. Even so the vibronic resonances remain essentially isolated. The weak interaction between two multiplicities allows us to move from the dynamics of adiabatic states to the dynamics of vibronic states of definite multiplicity. To do that, we transfer from adiabatic electronic states to the vibronic basis using the eigenvectors $X_{\nu,g,n}$ where $\nu$ is the vibrational index and $n$ is the index of the singlet electronic states and $g$ is the site on the internuclear distance grid. The resulting amplitude of the $\nu$'th vibronic state is $A_\nu(t)$ given by:

$$A_\nu(t) = \sum_{g=1}^{Ng} \sum_{n=1}^{Ne} C_{g,n}(t) X_{\nu,g,n} \qquad (3)$$

$C_{g,n}(t)$ are time-dependent amplitudes of the wave function of state *n* at a grid point *g* propagated for *Ne* singlet electronic states on a grid consisting of *Ng* points. The resulting population of each vibronic state ν, $P_\nu(t)$, is calculated via the amplitudes $A_\nu(t)$:

$$P_\nu(t) = A_\nu^*(t)A_\nu(t) \tag{4}$$

and the coherence between different ν and ν ' states, $B_{\nu,\nu'}(t)$, is computed as:

$$B_{\nu,\nu'}(t) = A_\nu^*(t)A_{\nu'}(t) \tag{5}$$

Fig. 2a shows population of vibronic states of the singlets $P_\nu(t)$ at 60 fs when the fast pulse is just over. The states with the highest weights are at the vibronic quantum numbers $\nu_{15}$ – $\nu_{20}$ and their distribution is what one would expect from excitation in the Franck-Condon region, see also Fig. S6 of SM. This is unchanged when we increase the strength of the pulse. We next discuss the more populated vibronic states in detail. These states decay very slowly in time (Fig. 2b) and their vibronic coherence is oscillating (Fig. 2c and Fig. S7 of the SM). Relatively slow linear decay caused by dissociation can be seen in Fig. 2b for the states $\nu_{18}$ and $\nu_{19}$ while for other states the population's loss is not even evident to a graph reading accuracy. By using a logarithmic plot of the populations, Fig. 2d, one determines the predissociation rate of each vibronic state as the slope of the straight line. Using the rates, one can extrapolate the exponential decay of the population to longer times. Fig. 3 shows the decay of the overall excited singlet states, $P_S$(t), and vibronic states ν = 15-21.

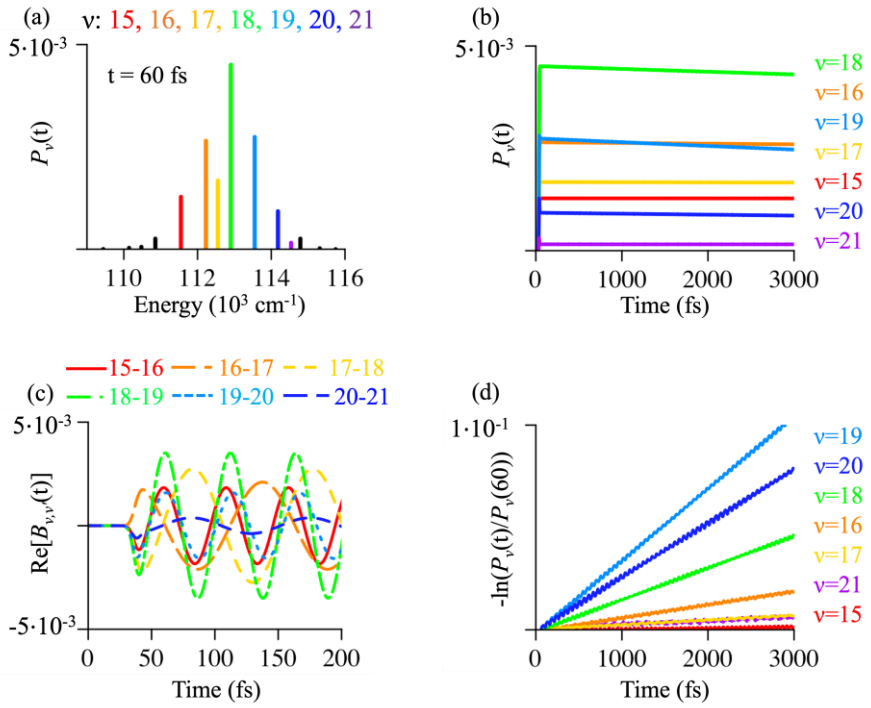


FIG. 2. (a) Population of all the vibronic singlet states of ${}^1\Sigma_u^+$ symmetry excited by an ultrafast pulse. Vibronic levels that are shown in color, ν =15-20, have the higher weight, so (b) and (c) demonstrate the time dependence for population, $P_\nu(t)$ (b), and coherence, $B_{\nu,\nu'}(t)$ (c), between these particular states only. The vibrational quantum number is essentially a good one because these vibronic states also diagonalize the nonadiabatic couplings. The color code in panel (c) shows the coherence between states $\nu$ and $\nu'$. (d) The logarithmic plot of the population decay during 3 ps after the pulse is over. The slight wiggles in (d) are due to the transfer of amplitudes from the singlets to the triplets that is non monotonic in time nor is it uniform along the grid. In other words, the decay on a logarithmic scale is almost a staircase function reflecting the localized along the grid transfer from singlets to triplets. See the movie S1 in the SM.

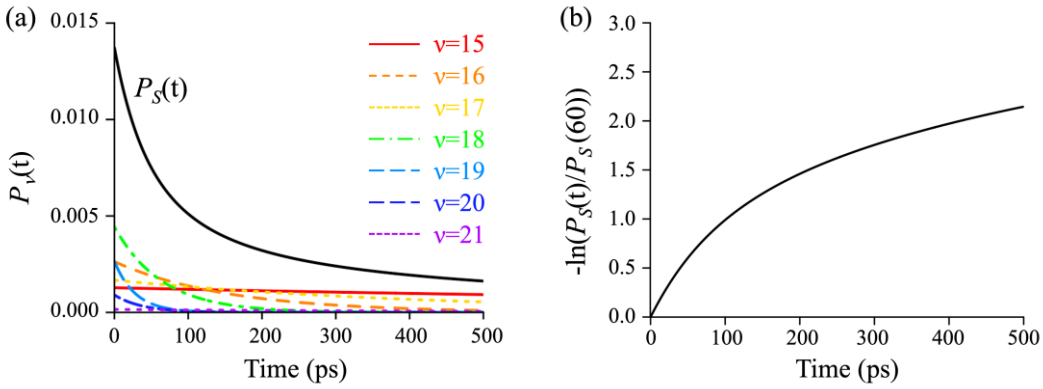

FIG. 3. (a) Decay of the overall excited singlet states population $P_S$(t) extrapolated to longer times, in black. The contributions of the vibronic components are color coded. (b) The initial fast exponential decay rate changes to a slower decay at longer times. The faster decay is due to the states $\nu$ = 18,19 and 20 that are coupled to a repulsive triplet $2^3\Pi_u$ exit channel. The respective predissociation lifetimes are given in Table 1.

The lifetime of each vibronic state in the coherent superposition is obtained by taking the inverse of the predissociation rate. The computed predissociation lifetimes of the vibronic levels 15-20 are given in Table 1. We compare these lifetimes with the lifetimes computed for an excitation of isolated vibronic states by an ultraslow laser pulse. These are computed using the same Hamiltonian, grid, and time spacings. The individual state dynamics is carried out with well-defined narrow laser pulses of total width of 200 $cm^{-1}$ which allows accessing a single vibronic level. The duration of the pulse is far longer than the period of the coherence of the electronic singlets. Hence, in contrast to the situation for the ultrafast excitation, see Fig. S8, we do not see the beating of the electronic coherence.

Excited isolated vibronic states decay exponentially, each with its own lifetime as shown in Table 1. These lifetimes are fully consistent with values reported previously for computations with a larger electronic basis set. The electronic basis used here is those states that are primarily involved in the dynamics as listed in Table I of [29].

Reported experimental singlet's lifetimes are also shown in Table 1. Apart from the very long-lived state there is a quite good agreement.

Table 1. Predissociation lifetime $\tau_{diss}$ computed for singlet states population decay followed upon the ultrafast (coherent) and ultraslow (incoherent) [29] excitation along with the experimentally measured lifetimes. In the case of the ultrafast excitation, the lifetime is computed using the results shown in Fig. 2d.

| *v* | $E_v$, $cm^{-1}$ | $\tau_{diss}$, *ps* | | *Experimental τ, ps* |
|---|---|---|---|---|
| | | *coherent* | *incoherent* | |
| 15 | 111,549 | 1541 | 1535 | 250 [52] |
| 16 | 112,226 | 154 | 154 | 250 [52] |
| 17 | 112,551 | 443 | 440 | 340 [53] |
| 18 | 112,903 | 64 | 64 | 74 [53] |

| | | | | |
|---|---|---|---|---|
| 19 | 113,551 | 28 | 28 | 28 [54] |
| 20 | 114,182 | 38 | 38 | 31 [54] |
| 21 | 114,538 | 496 | 535 | – |

As seen in Table 1 the lifetime of the singlets varies in a not quite monotonic way with the energy of excitation. This is a reflection of the entangled dynamics in the triplet manifold. In this energy range there are two exit channels that correspond to different triplet states. The relative branching between the two exits varies in a similar non-monotonic way with energy. To demonstrate the different dynamics at different energies we plot in Fig. 4 the results of the computed separately at three different energies with a long pulse. Shown are the populations along the grid for either singlets, upper panels, or triplets. The longer lifetime at $\nu$ =17 is due to a weaker coupling between the Rydberg singlet and triplet at short internuclear distances, Fig. 4a. The fast decay of $\nu$ =18-20 (shown in Fig. 4b is $\nu$ =19) is due to an effective exit through a repulsive $2^3\Pi_u$ state. The slow decay of $\nu$ =21 is due to an effective trapping at the $3^3\Pi_u$ state, see Fig. 4c. Excitation by a short pulse creates a coherent superposition of these states with a complex dynamics as seen in the movie S1 of the SM. At the time of 61 fs therein there is a fast transfer from a singlet to a triplet repulsive potential. Around 91 fs one sees the transfer between the Rydberg states localized at a short distance. Snapshots at these two times are also shown in Fig. S9 of the SM. These non-monotonic in time exits are seen as the steps in the logarithmic decay of the populations.

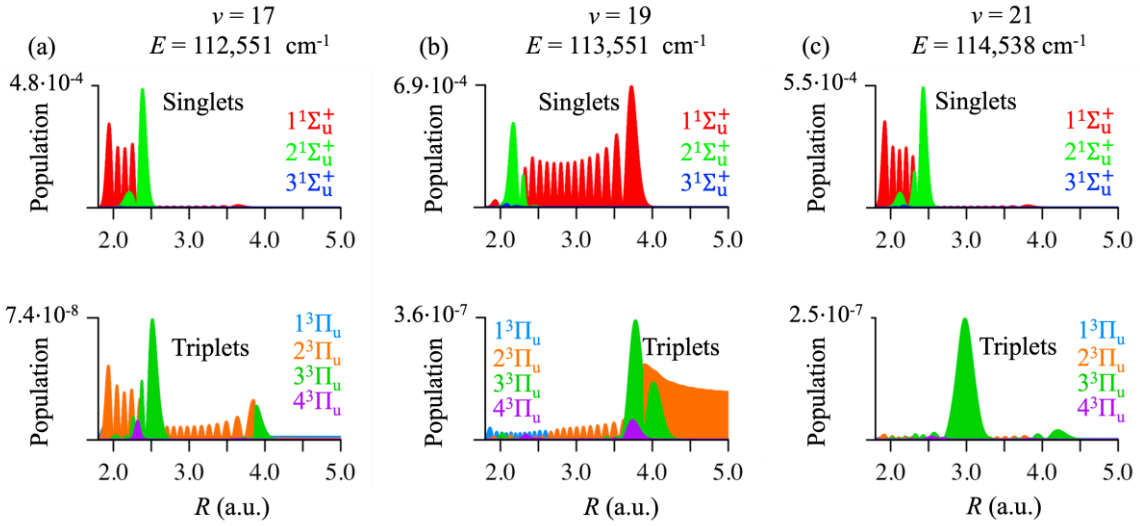


FIG. 4. The portraits of the dynamics at three different energies computed for excitation by a long pulse: (a) at 112,551 cm$^{-1}$, (b) at 113,551 cm$^{-1}$ and (c) 114,538 cm$^{-1}$. Upper/lower panels:

Population in the singlets/triplets along the internuclear distance. Adiabatic electronic states are color coded.

The dissociation lifetimes obtained from both types of excitation are close and so do not show any noticeable effect of interference between the coherently excited vibronic states [30]. To elucidate the role of spin-orbit coupling, we performed a simple computational test by increasing *in silico* the strength of the coupling between all triplet and singlet states by an order of magnitude and then even by two orders. Fig. 5a depicts the monoexponential photodissociation decay when the coupling is small. Each vibronic state decays in a unimolecular manner with its own rate. A larger spin-orbit coupling changes the predissociation rate and the wiggles due to the population transfer, Fig. 5b. The weights of the states in the eigenstates are shown in Fig. S5b and S5c of the SM. A further increase of the spin-orbit coupling makes for a very fast dissociation and even the order of preferable exit channels changes, Fig. 5c.

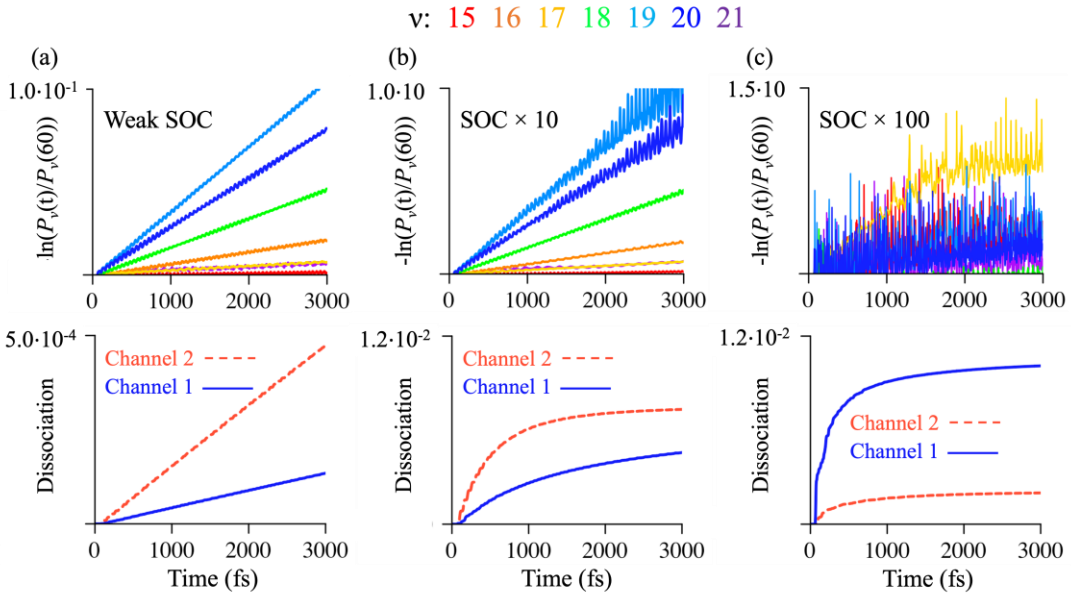


FIG. 5. The logarithmic plot of the singlet state population decay in the vibronic levels 15-20 (top panel) and overall dissociation into Channels 1 and 2 (bottom panel) during the ultrafast pulse induced dynamics. The dissociation is calculated as a population of triplet states absorbed by a complex potential at $R > 6.2$ a.u. [38]. (a) Dynamics computed for a weak spin-orbit coupling of $N_2$, and then *in silico* increasing the spin-orbit coupling between the singlet and triplet states by a factor of (b) 10 and (c) 100; the color code the same as in Figure 2d.

## IV.CONCLUDING REMARKS

We discussed dissociation from a large manifold of states through a narrow bottleneck. The unusual feature is that the bottleneck is not in the exit region towards the free products but at a pre-dissociative early spin-orbit coupling regime as seen in Fig. 1. Quantum dynamical simulations based on high-level quantum chemical potentials, nonadiabatic and spin-orbit couplings show, Fig. 2, that a fast VUV pulse excites coherently different vibronic singlet states of $N_2$. The dynamics show that following a fast coherent excitation these vibronic states dissociate essentially independently of one another as is to be expected for isolated resonances. Using a long pulse the simulations show that the very same vibronic states can be individually excited and that their population decay times are largely the same as for the coherent excitation. The state coherently excited by a fast pulse decays as an incoherent mixture of the vibronic states as seen in Fig. 3. The non-monotonic variation of the decay time as seen in Table 1 is interpreted in Fig. 4. The effects of coherence can be seen but only for an artificially much stronger spin-orbit coupling, Fig. 5 or for a probe that is phase sensitive.

ACKNOWLEDGMENTS

The authors thank the referees for their critical comments and fruitful suggestions. The authors acknowledge financial support by the US–Israel Grant, No. 2019722 NSF–BSF Astronomy and Astrophysics. FR acknowledges the support of the Fonds National de la Recherche (F.R.S.-FNRS, Belgium), #T0205.20.

REFERENCES

[1] W. S. Warren, J. B. Murdoch, and A. Pines, J Magn Reson **60**, 236 (1984).
[2] W. S. Warren, D. P. Weitekamp, and A. Pines, J Chem Phys **73**, 2084 (1980).
[3] T. Den, H. M. Frey, P. M. Felker, and S. Leutwyler, J Chem Phys **143**, 144306 (2015).
[4] P. Benharash, M. J. Gleason, and P. M. Felker, J Phys Chem A **103**, 1442 (1999).
[5] S. D. Chao, H. L. Selzle, H. J. Neusser, E. W. Schlag, L. Yao, and S. H. Lin, Zeitschrift Fur Physikalische Chemie **221**, 633 (2007).
[6] A. Held and E. W. Schlag, Accounts Chem Res **31**, 467 (1998).
[7] J. Zheng, K. Kwak, and M. D. Fayer, Accounts Chem Res **40**, 75 (2007).
[8] D. W. McCamant, P. Kukura, and R. A. Mathies, J Phys Chem B **109**, 10449 (2005).
[9] A. H. Zewail, Angew Chem Int Edit **40**, 4371 (2001).
[10] K. B. Moller, N. E. Henriksen, and A. H. Zewail, J Chem Phys **113**, 10477 (2000).
[11] M. Bixon, J. Jortner, and Y. Dothan, Mol Phys **17**, 109 (1969).
[12] E. R. Warrick, J. E. Baekhoj, W. Cao, A. P. Fidler, F. Jensen, L. B. Madsen, S. R. Leone, and D. M. Neumark, Chem Phys Lett **683**, 408 (2017).
[13] E. R. Warrick, W. Cao, D. M. Neumark, and S. R. Leone, J Phys Chem A **120**, 3165 (2016).
[14] E. Goulielmakis *et al.*, Nature **466**, 739 (2010).

[15] K. G. Komarova, F. Remacle, and R. D. Levine, J Chem Phys **151**, 114308 (2019).
[16] J. S. Ajay, K. G. Komarova, S. Van den Wildenberg, F. Remacle, and R. D. Levine, in *Rsc Theor Comput Che*, edited by M. J. J. Vrakking (The Royal Society of Chemistry, Cambridge, UK, 2018), pp. 308.
[17] B. R. Lewis, A. N. Heays, S. T. Gibson, H. Lefebvre-Brion, and R. Lefebvre, J Chem Phys **129**, 164306 (2008).
[18] H. Lefebvre-Brion and B. R. Lewis, Mol Phys **105**, 1625 (2007).
[19] M. Lucchini, K. Kim, F. Calegari, F. Kelkensberg, W. Siu, G. Sansone, M. J. J. Vrakking, M. Hochlaf, and M. Nisoli, Phys Rev A **86**, 043404 (2012).
[20] D. Spelsberg and W. Meyer, J Chem Phys **115**, 6438 (2001).
[21] W. C. Ermler, A. D. Mclean, and R. S. Mulliken, J Phys Chem-Us **86**, 1305 (1982).
[22] J. S. Ajay, K. G. Komarova, F. Remacle, and R. D. Levine, P Natl Acad Sci USA **115**, 5890 (2018).
[23] A. R. Beck, D. M. Neumark, and S. R. Leone, Chem Phys Lett **624**, 119 (2015).
[24] R. D. Levine, *Quantum mechanics of molecular rate processes* (Clarendon P, Oxford, 1969).
[25] F. Remacle, M. Munster, V. B. Pavlovverevkin, and M. Desouterlecomte, Phys Lett A **145**, 265 (1990).
[26] F. Remacle and R. D. Levine, Mol Phys **87**, 899 (1996).
[27] J. P. Sprengers, A. Johansson, A. L'Huillier, C. G. Wahlstrom, B. R. Lewis, and W. Ubachs, Chem Phys Lett **389**, 348 (2004).
[28] M. O. Vieitez, T. I. Ivanov, W. Ubachs, B. R. Lewis, and C. A. de Lange, J Mol Liq **141**, 110 (2008).
[29] N. Gelfand, K. Komarova, F. Remacle, and R. D. Levine, Astrophys J **948**, 58 (2023).
[30] T. Grinev and P. Brumer, J Chem Phys **143**, 244313 (2015).
[31] L. A. Pachon and P. Brumer, Phys Rev A **87**, 022106 (2013).
[32] F. Fassioli, A. Olaya-Castro, and G. D. Scholes, J Phys Chem Lett **3**, 3136 (2012).
[33] A. Chenu, A. M. Branczyk, G. D. Scholes, and J. E. Sipe, Phys Rev Lett **114** (2015).
[34] P. Jiang, L. Y. Lu, M. Liu, and H. Gao, Phys Chem Chem Phys **24**, 11544 (2022).
[35] M. Liu, P. Jiang, L. Y. Lu, T. H. Yin, L. Y. Ma, M. Cheng, Q. Z. Yin, and H. Gao, Astrophys J **923**, 196 (2021).
[36] M. Liu, P. Jiang, M. Cheng, and H. Gao, J Chem Phys **155**, 234305 (2021).
[37] F. H. Lefebvre-Brion, R.W. Field *The Spectra and Dynamics of Diatomic Molecules* (Academic Press, San Diego, 2004), p. 786.
[38] N. Gelfand, K. Komarova, F. Remacle, and R. D. Levine, J Chem Phys **158**, 164302 (2023).
[39] P. J. Knowles and H. J. Werner, Chem Phys Lett **115**, 259 (1985).
[40] H. J. Werner and P. J. Knowles, J Chem Phys **82**, 5053 (1985).
[41] D. A. Kreplin, P. J. Knowles, and H. J. Werner, J Chem Phys **150** (2019).
[42] P. J. Knowles and H. J. Werner, Chem Phys Lett **145**, 514 (1988).
[43] H. J. Werner, B. Follmeg, and M. H. Alexander, J Chem Phys **89**, 3139 (1988).
[44] D. Simah, B. Hartke, and H.-J. Werner, J. Chem. Phys. **111**, 4523 (1999).
[45] A. Berning, M. Schweizer, H.-J. Werner, P. J. Knowles, and P. Palmieri, Mol. Phys. **98**, 1823 (2000).
[46] G. K. H.-J. Werner; P. J. Knowles, F. R. Manby, M. Schutz, P. Celani, W. Gyorffy, D. Kats, T. Korona, R. Lindh, A. Mitrushenkov, G. Rauhut, K. R. Shamasundar, T. B. Adler, R. D. Amos, A. Bernhardsson, A. Berning, D. L. Cooper, M. J. O. Deegan, A. J. Dobbyn, F. Eckert, E. Goll, C. Hampel, A. Hesselmann, G. Hetzer, T. Hrenar, G. Jansen, C. Koppl, Y. Liu, A. W. Lloyd, R. A. Mata, A. J. May, S. J. McNicholas, W. Meyer, M. E. Mura, A. Nicklass, D. P.

O'Neill, P. Palmieri, D. Peng, K. Pfluger, R. Pitzer, M. Reiher, T. Shiozaki, H. Stoll, A. J. Stone, R. Tarroni, T. Thorsteinsson, and M. Wang, MOLPRO, a package of ab initio programs, 2015.
[47] A. Hofmann and R. de Vivie-Riedle, Chem. Phys. Lett. **346**, 299 (2001).
[48] F. T. Smith, Phys. Rev. **179**, 111 (1969).
[49] M. Baer, *Beyond Born-Oppenheimer: electronic nonadiabatic coupling terms and conical intersections* (Wiley, Hoboken, New Jersey, 2006), p.^pp. 26-57.
[50] T. Pacher, L. S. Cederbaum, and H. Köppel, in *Adv. Chem. Phys.*1993), pp. 293.
[51] W. H. Press, S. A. Teukolsky, W. T. Vetterling, and B. P. Flannery, *Numerical Recipes in Fortran 77: the Art of Scientific Computing. 2nd ed.* (Cambridge University Press, Cambridge, 1996).
[52] H. Oertel, M. Kratzat, J. Imschweiler, and T. Noll, Chem Phys Lett **82**, 552 (1981).
[53] H. Helm, I. Hazell, and N. Bjerre, Phys Rev A **48**, 2762 (1993).
[54] A. N. Heays, B. R. Lewis, G. Stark, K. Yoshino, P. L. Smith, K. P. Huber, and K. Ito, J Chem Phys **131** (2009).